Sensitivity of East Asian Summer Monsoon Precipitation to the Location of the Tibetan Plateau

SOO-HYUN SEOK[a] AND KYONG-HWAN SEO[a,b]

[a] *Department of Atmospheric Sciences, Division of Earth Environmental System, Pusan National University, Busan, South Korea*
[b] *Research Center of Climate Sciences, Pusan National University, Busan, South Korea*

(Manuscript received 23 February 2021, in final form 13 July 2021)

ABSTRACT: Recent studies have highlighted that a primary mechanism of the East Asian summer monsoon (EASM) is the fluid dynamical response to the Tibetan Plateau (TP), that is, orographically forced Rossby waves. With this mechanism in mind, this study explores how changes in the location of the TP affect the EASM precipitation. Specifically, the TP is moved in the four cardinal directions using idealized general circulation model experiments. The results show that the monsoon aspects are entirely determined by the location of the TP. Interestingly, the strongest EASM precipitation occurs when the TP is situated near its current location, a situation in which downstream southerlies are well developed from the surface to aloft. However, southerlies into the EASM region weaken as the TP moves, which in turn reduces the precipitation. Nevertheless, as long as it moves in the east–west direction, the TP is likely to force the stationary waves that induce precipitation over the midlatitudes (not necessarily over East Asia). In contrast, moving the TP well north of its original location does not induce strong monsoon flows over the EASM region, resulting in the driest case. Meanwhile, although the southward movement of the TP triggers downstream southerlies to some extent, it does not lead to an increase in the precipitation. Overall, these results show that the location of the TP is crucial in determining the EASM precipitation, and the latter is much more sensitive to the displacement of the TP in the meridional direction than in the zonal direction.

KEYWORDS: Monsoons; Climate variability; Climate variability

1. Introduction

The Tibetan Plateau (TP) was formed as a result of the collision between the Indian subcontinent and Eurasia (Molnar et al. 1993). Previous studies pointed out that this tectonic event triggered a significant shift in the climate system (Hahn and Manabe 1975; Manabe and Broccoli 1990; Kutzbach et al. 1993). For example, the East Asian summer monsoon (EASM) underwent considerable changes due to the uplift on geological time scales, including its intensity and variability (An et al. 2001). The TP currently still plays a crucial role in the formation and evolution of the EASM, and many studies have investigated the associated physical mechanism. The EASM is thought to be a subtropical monsoon (or hybrid type of tropical and subtropical monsoon), where seasonal wind reversals primarily appear (Ding and Chan 2005). One of the distinct features of the EASM is the southwest–northeast elongated rainband extending from eastern China to the Korean Peninsula and Japan (Fig. 1).

To investigate the effect of the TP on the EASM, some studies conducted numerical experiments that progressively change the height of the TP (Liu and Yin 2002; Abe et al. 2003; Lee et al. 2015). Kitoh (2004) reported that the EASM-like rainband pattern can appear when the mountain height is over 60% of its original height. According to that study, the uplift of the TP strengthens both the North Pacific subtropical high (NPSH) and southwesterly flow from the Indian Ocean, leading to an increase in precipitation over the EASM region. However, when the mountain height exceeds 100% of its original, the intensified subtropical high is more important than the monsoonal southwesterly in transporting moisture toward the Asian continent. Herein, we can infer that the NPSH is crucial to the EASM and may be related to large-scale orography such as the TP (Rodwell and Hoskins 2001; Miyasaka and Nakamura 2005; Duan et al. 2017).

Some studies concentrated on the seasonal evolution of the upper-tropospheric subtropical westerly jet, which is the key to understanding the drastic alternation of humid and arid climates in East Asia. For example, Zhang et al. (2006) stated that the zonal location change in the jet core is involved in determining heavy summer rainfall over East Asia. On the other hand, Lin and Lu (2008) emphasized that the westerly jet undergoes the meridional migration over East Asia, concurring with the onset and withdrawal of the EASM. Park et al. (2012) also described that the TP induces a zonally asymmetric rainfall pattern with downstream convergence during the late spring and early summer, when the westerly jet still resides over the southern TP, consequently affecting the EASM. Furthermore, Sato (2009) presented the dynamic and thermal effects of the TP depend mainly on the seasonal variation in the westerly through a regional climate model.

Meanwhile, Ringler and Cook (1995) conducted a series of experiments with a mountain placed at 0°, 15°, 30°, 45°, and 60°N and found that thermal and mechanical effects vary with mountain features such as its location, which in turn control stationary wave patterns. In addition, they demonstrated that orographically forced stationary waves must be analyzed within a nonlinear framework because the interaction between thermal and mechanical forcing makes the total response not equal to the sum of the individual responses (Ringler and Cook 1999). These results suggest the difficulty in distinguishing between the thermal and mechanical effects of the TP.

Nevertheless, many recent studies have emphasized the importance of the mechanical effect of the TP associated with

Corresponding author: Dr. Kyong-Hwan Seo, khseo@pusan.ac.kr

DOI: 10.1175/JCLI-D-21-0154.1

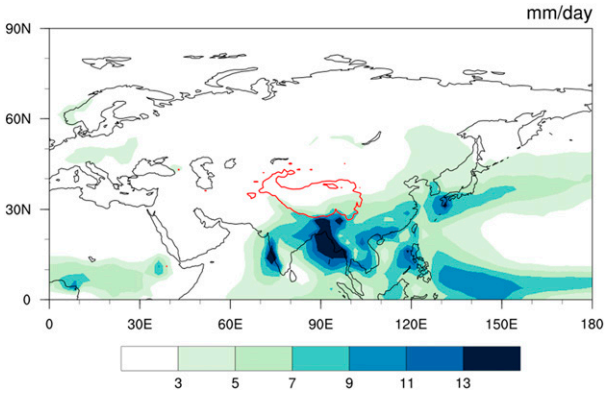

FIG. 1. GPCP climatological (1991–2020) June–July mean precipitation. The red contours represent 3000-m elevation.

the westerly jet in explaining the EASM (Sampe and Xie 2010; Son et al. 2019, 2020; Chiang et al. 2020; Kong and Chiang 2020). Sampe and Xie (2010) highlighted that the horizontal warm air advection from the eastern TP by the midtropospheric westerly increases atmospheric instability downstream, which is conducive to an ascending motion over the EASM region.

Next, Kong and Chiang (2020) revealed the relationships among the extratropical northerlies, the meridional position of the jet, and the mei-yu stage. They showed that as the upper-tropospheric westerly jet shifts northward with its seasonal transition, the meridional gradient of equivalent potential temperature $-\partial\theta_e/\partial y$ weakens along with a reduction in the downstream northerly over central China. Note that the strong gradient of θ_e represents boundaries of air masses with different properties in temperature or moisture, where θ_e is considered a useful variable for analyzing frontal monsoon systems (Seo et al. 2011, 2015). In addition, they found that when the westerly jet moves northward over the northern edge of the TP, it leads to the demise of the mei-yu front.

Chiang et al. (2020) recently reported that the distinct rainfall stages in East Asia (spring, pre-mei-yu, mei-yu, midsummer, and fall) can be attributed to the position of the subtropical jet and its interaction with the TP. Interestingly, they highlighted that the meridional transition of the westerly jet modulates the extratropical northerlies over northeastern China, which consequently leads to the aforementioned various rainfall stages. In other words, the TP-induced northerlies determine the strength and meridional positioning of the rainfall, restricting the lower-level monsoonal southerlies from expanding to the mei-yu region. However, as summer progresses (and thus the jet moves northward), the rainband gradually moves to the north and disappears with the reduced northerlies, which is consistent with Kong and Chiang (2020), as introduced in the previous paragraph.

In the meantime, Son et al. (2019) used idealized numerical model simulations [as previously done in Chou (2003), Liu et al. (2007), and Wu et al. (2007, 2012)] to reveal the relative contribution of each factor affecting the EASM precipitation by isolating the role of individual physical processes. According to their study, the upstream westerly jet impinging on the TP triggers barotropic Rossby waves, which consequently induces the downstream southerlies between the trough over the continent and the ridge over the ocean (see Fig. 5 in Son et al. 2019). They accentuated the pure dynamical impact of the TP, which explains about 70% of the EASM precipitation, despite the weaker jet stream in summer than in winter. However, determination of the most important factor in the EASM generation still remains controversial (Wang et al. 2008; Molnar et al. 2010; Wu et al. 2012; Chen et al. 2014).

In addition, the downstream wave response due to the TP can account for the seasonal evolution of monsoonal precipitation over East Asia. Based on the barotropic Rossby wave theory, Son et al. (2020) calculated the zonal gradient of geopotential height and showed that the EASM rainband moves zonally along with the strong gradient region characterized by intense moist advection by southerlies from the low latitudes. Moreover, they presented that the westerly jet speed in the upstream region is the key to explaining the zonal migration of the EASM rainband. Therefore, we can infer that the area where the southerlies induced by the orographic forcing prevail is largely consistent with the location of the rainband.

From these previous studies (e.g., Lin and Lu 2008; Son et al. 2019, 2020; Chiang et al. 2020), it is plausible that the relative position of the jet stream to the TP (and thus the speed of the incident westerly wind) is regarded as a crucial factor, which is responsible for the EASM (intra)seasonality and variability. Recent studies even conducted model simulations that reshape the TP (not just change the height) to explore the link between the orography and the EASM (Chen et al. 2014; Baldwin and Vecchi 2016; Kong and Chiang 2020). However, while many model experiments have adjusted the shape or height of the TP, the importance of its location has been relatively overlooked. Thus, we aim to explore the dependency of the EASM precipitation on the location of the TP by moving it in the four cardinal directions. For a simple and clear interpretation, we conduct atmospheric general circulation model (AGCM) experiments with simplified boundary conditions.

The remainder of this paper is organized as follows. In section 2, we describe the model and dataset used in this study. Section 3 provides an overview of the influence of the TP on the EASM using a series of height change experiments. We then demonstrate the changes in the EASM precipitation based on the relocation of the TP. A summary and discussion are provided in section 4.

2. Model, experimental design, and data

To perform our analysis, we utilized the Geophysical Fluid Dynamics Laboratory (GFDL) Atmosphere Model, version 2.1 (AM2.1; Anderson et al. 2004). AM2.1 uses a finite-volume dynamical core (Lin 2004) with a horizontal grid spacing of 2.5° longitude by 2.0° latitude and 24 vertical levels. We also used precipitation data on a 2.5° × 2.5° longitude–latitude grid for the period 1991–2020 from the Global Precipitation Climatology Project (GPCP) (Adler et al. 2003).

In this study, we designed a series of experiments with highly idealized boundary conditions to provide a simple framework. First, a flat continent is located over 20°–120°E and 15°–70°N

and a Gaussian bell-shaped mountain is embedded into the continent, representing the Eurasian continent and the TP, respectively. We assumed that the original TP is centered at 35°N, 80°E, with a maximum height of 5 km, and a half-width of (30°, 10°) in longitude and latitude. For a simple ocean boundary condition, monthly climatological zonal mean sea surface temperatures (SSTs) were specified. The SSTs were obtained from the NOAA Optimum Interpolation sea surface temperature V2 (Reynolds et al. 2002). In addition, the ground surface was assumed to be covered with grass, and the grass albedo is 0.18. This experiment is the control run (CTR) illustrated in Fig. 2, and it has been shown to simulate well the realistic thermodynamic and dynamic fields associated with the EASM (Son et al. 2019).

Having introduced CTR, we now move the TP on the continent and name these experiments as TPE10, TPW10, TPW20, . . . , TPS10. For example, TPE10 refers to the experiment in which the TP is located 10° east from that in CTR. The land-only experiment, NoTP, was also conducted to compare responses to the presence of the TP in each case. All runs were integrated for 12 years, and the last 10 years were used for the analysis. Each experiment consisted of five ensemble members made by small fluctuations to an atmospheric initial condition. Furthermore, additional runs were performed to analyze the development of the EASM according to the TP height, which are named TPH08, TPH06, THP04, and TPH02. Here, TPH08 represents the experiment in which the TP height is 80% of that in CTR. In each model integration, the boundary conditions such as SSTs remain almost the same except for the orography. All results are averaged over June–July. Through comparing AGCM and atmosphere–ocean coupled model simulations, several studies revealed that orographic changes modify SST distribution through air–sea interaction (Kitoh 2004; Okajima and Xie 2007). Nevertheless, we opted to use the AGCM (i.e., AM2.1) because the previous simulations (e.g., Son et al. 2019) skillfully reproduced the characteristic features of the EASM, including the slanted rainband. Moreover, using the AGCM facilitates the controls of various experimental conditions and parameters, making it easier to examine their sensitivity.

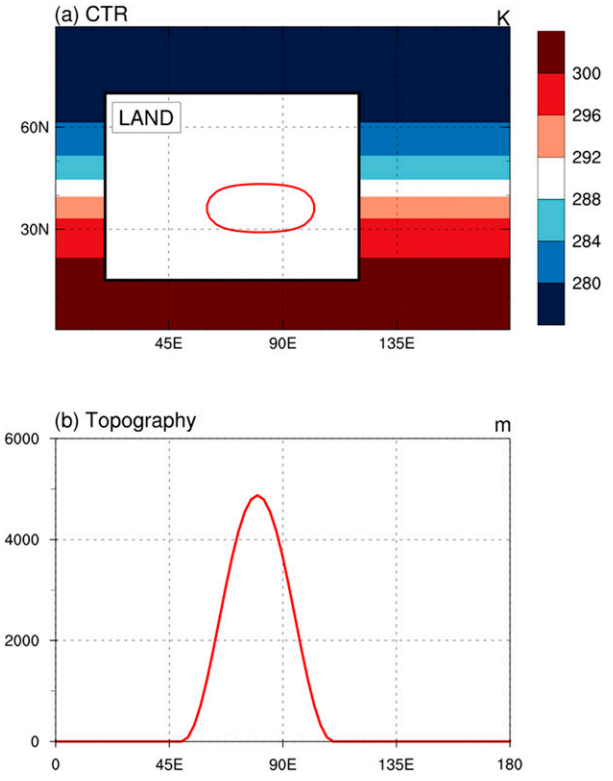

FIG. 2. Experimental design of the control run (CTR). (a) SST (shaded; K). The black contour denotes the continent boundary, and the red isoline is 1000-m elevation. (b) Topographic elevation (m) along 35°N.

3. Results

a. *Barotropic wind structure induced by the TP*

As the monsoon season approaches, the NPSH extends westward to generate a strong zonal pressure gradient in the EASM region (Son et al. 2020), inducing a burst of southerly flows. This condition helps to maintain the EASM precipitation because the southerlies transport heat and moisture from the low latitudes to the midlatitudes. In fact, many studies accentuated that the southerlies, specifically forced by the TP, are essential for the generation of the EASM (Ding and Chan 2005; Sampe and Xie 2010; Chen and Bordoni 2014; Son et al. 2019, 2020). In this regard, before examining the simulation results related to the TP location, we briefly analyze the development of the winds according to the TP height.

Figure 3 shows precipitation and vertically integrated moisture flux pattern with respect to the uplift of the TP. The EASM domain (110°–140°E, 30°–40°N) is marked by the blue box from Fig. 3 onward. Herein, the vertically integrated moisture flux (VIMF) is calculated as

$$\mathrm{VIMF} = -\frac{1}{g}\int_{p_s}^{300\,\mathrm{hPa}} q\mathbf{V}\,dp, \tag{1}$$

where g is the gravitational acceleration, p_s is surface pressure, q is specific humidity, $\mathbf{V}$ is wind vector, and p is pressure. In addition, a linear regression is performed on precipitation at each grid point, which follows the equation

$$Y = \alpha + \beta X, \tag{2}$$

where Y is the precipitation, X is a set of the uplift values, and α and β are the regression coefficients. Here X has values of 0, 2, 4, 6, 8, and 10, representing the uplift level. For example, the uplift value corresponding to THP02 is 2. That is, β represents the sensitivity of precipitation to the extent of uplift (Fig. 3a).

Based on Fig. 3a, the precipitation pattern becomes asymmetric with increasing TP height because it triggers rainfall in the downstream region. Particularly, the response is conspicuous in the southeastern TP and the EASM region. It is interesting to note that the rainband starts to appear in TPH06, which is generally consistent with Kitoh (2004). In TPH08, the overall precipitation pattern and intensity are approximately

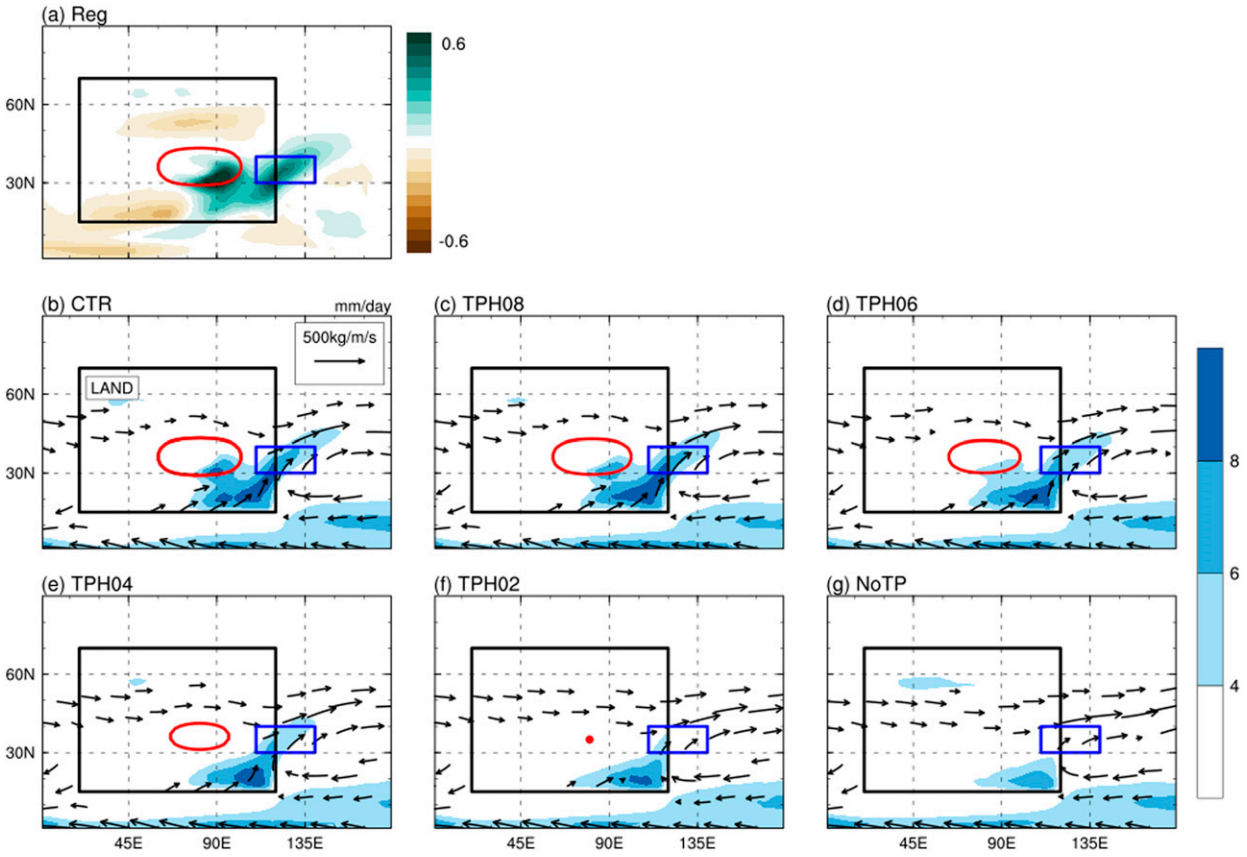

FIG. 3. (a) Regressed precipitation on the uplift values. The actual increase in precipitation values from NoTP (i.e., $X = 0$) to CTR (i.e., $X = 10$) is approximately 10 times the regression field shown in the plot. (b)–(f) Distribution of precipitation (shaded; mm day^{-1}) and vertically integrated (from p_s to 300 hPa) moisture flux (vectors; kg m^{-1} s^{-1}). The red isoline is 1000-m elevation in each experiment. The EASM domain (110°–140°E, 30°–40°N) is enclosed by the blue box. Magnitude of vectors less than 150 kg m^{-1} s^{-1} is omitted.

the same as those in CTR. Conversely, the rainband is not captured when the TP is removed (Fig. 3g). These results imply that to reproduce the precipitation shown in CTR, the height of the TP should be at least 80% of the original height. In fact, many studies reported that the precipitation gradually increases as the TP rises to a certain height (Abe et al. 2003; Kitoh 2004; Lee et al. 2015). Furthermore, an increase in precipitation over the EASM region seems to always accompany moisture transport from the low latitudes (Figs. 3b–g). This again emphasizes that the TP height is a critical modulator of the EASM precipitation associated with the southerly flows.

Of note is that the South Asian summer monsoon-like precipitation pattern is likely to appear due to the land–sea distribution even without the TP (Liu and Yin 2002; Lee et al. 2015), but there exists only a small amount of precipitation in that region for NoTP (Fig. 3g). This is probably because we imposed the square land to simply mimic the Eurasian continent without including the landmasses of Africa, India, and the Indochina Peninsula. Wu et al. (2012) showed that when the three tropical lands are included along with the Eurasian continent, an intense rain belt extends from Africa to the South China Sea through the interaction between the tropics and subtropics. Indeed, a simulation with a more realistic (but still simple) configuration including Africa and the Indian subcontinent produces a fair amount of precipitation even without the TP (not shown), which will be detailed in a future study.

Next, we examine the change in southerlies flowing into the EASM domain (Fig. 4). As described above, moisture provided by the southerlies is essential for the EASM precipitation. It seems that the uplift enhances the winds overall from the surface to aloft (Fig. 4a). The regression method used here is the same as the one used earlier, but it is for the meridional wind at 30°N instead of precipitation. It is also shown that the barotropic wind structure stands out in CTR (Fig. 4b). In contrast, only the weak monsoon flows, resulting from the land–sea thermal contrast (Wu et al. 2012), are simulated in NoTP (Fig. 4g). Therefore, we can confirm the production of the characteristic barotropic wind structure forced by the TP, as proposed by Son et al. (2019, 2020). In particular, the wind structure becomes evident in TPH08 (Fig. 4c), nearly identical to that in CTR. Note that the rainband shown in CTR is reproduced in TPH08, along with the development of the southerly winds. Here, the latitude of 30°N is chosen for the cross section because it is the southern boundary of the EASM

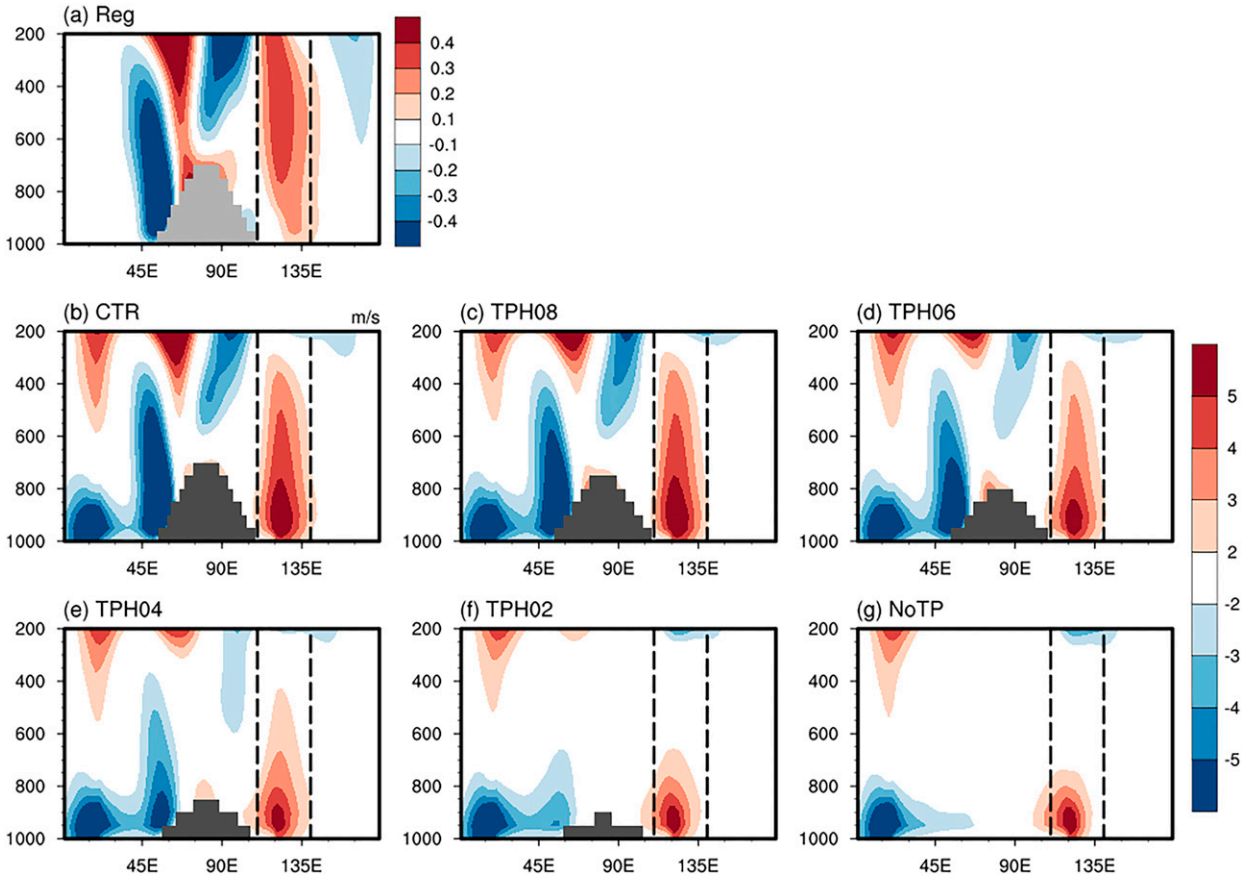

FIG. 4. Longitude–pressure cross section of (a) regressed meridional wind on the uplift values and (b)–(g) meridional wind (m s^{-1}) along 30°N. The thick vertical dashed lines denote the boundary of the EASM domain.

domain. We also evaluated the cross section at 35°N, but the characteristics of the wind did not change much (not shown).

b. Precipitation variation with the location of the TP

Figure 5 displays precipitation and 500-hPa eddy geopotential height (geopotential height deviation from the zonal mean) in all experiments. The southwest–northeast elongated rainband, which is one of the main features of the EASM, is evident in TPE10, TPW10, TPW20, and TPW30 as in CTR. Above all, the rainband stretches along the area where the zonal pressure gradient is prominent. In these cases, it seems that precipitation distribution is shifted sideways compared to that in CTR, and the same holds for pressure distribution. On the contrary, the precipitation pattern in TPN10 and TPN20 is not well distinguished from that in NoTP. This is also the case for TPS10, except that the southward movement of the TP causes heavy rainfall over the southern TP. Overall, when the TP moves northward or southward, a prominent pressure gradient does not appear in the EASM domain.

Figure 6 shows 850-hPa meridional wind and 200-hPa zonal wind. We first examine the change in precipitation patterns in terms of the southerly flow. The regions that exhibit vigorous southerlies correspond well to precipitation regions (see Figs. 5 and 6). This indicates that the southerlies are essential for the rainband, as stated earlier. For 200-hPa zonal wind, the jet core migrates with the movement of the TP in the east–west direction and is situated over the northern TP. The speed of the jet stream is also more zonally asymmetric than that in NoTP (Figs. 6a–f). In contrast, the jet does not directly cross over the orography in TPN10, TPN20, and TPS10 (Figs. 6g–i). The alteration in the westerly can be explained by the thermal wind balance, which is related to the surface heating over the TP.

Recent studies showed that the subtropical jet impinging on the TP controls the EASM precipitation (Molnar et al. 2010; Son et al. 2019, 2020; Chiang et al. 2020; Kong and Chiang 2020). Specifically, Son et al. (2020) considered the precipitation to be governed by the fluid dynamical response originating from potential vorticity conservation (Held 1983). They showed that orographic forced Rossby waves generate the strong pressure gradient over East Asia, inducing the southerlies and the EASM rainband. Based on this, the relative position of the westerly jet to the TP might account for the rainband and strong southerly flow appearing only in certain cases.

There is still a debate over the importance of the downstream southerlies in the EASM. For example, Son et al. (2019, 2020), underpinning our research, stressed the role of the southerly winds flow into the EASM region. However, Chiang et al. (2020) considered the TP-induced northerlies to be the

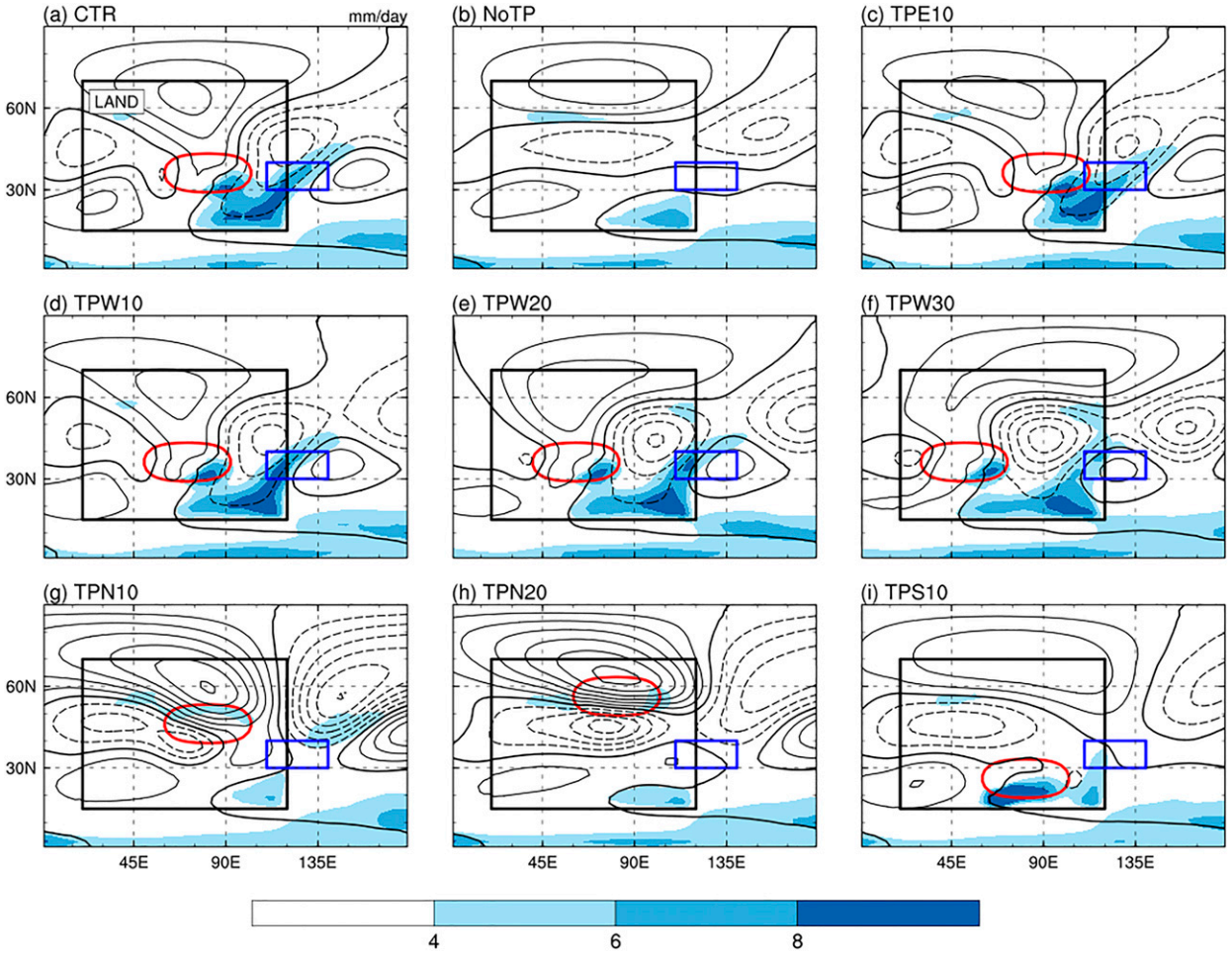

FIG. 5. Precipitation (shaded; mm day^{-1}) and 500-hPa eddy geopotential height (contour interval 20 gpm; solid for positive values and dashed for negative). The zero contour is thickened.

key to explaining the EASM and found that the southerlies result from land–sea distribution and diabatic heating induced by the rainband. This discrepancy appears to occur because they (i.e., Son et al. 2019, 2020; Chiang et al. 2020) analyzed different domains—Chiang et al. (2020) explored the relatively small area of 110°–120°E (125°E), while Son et al. (2020) examined a much wider area (i.e., 110°–160°E) following the stretched EASM rainband. In other words, the former is mainly for the analysis of mei-yu in China, while the latter provides a general perspective on the EASM rainband including the three components of the EASM (mei-yu, changma, and baiu).

In addition, we speculate the underlying mechanism does not differ much for Son et al. (2019, 2020) and Chiang et al. (2020), although their results seem to contradict. Through the Rossby wave response, ridges and troughs develop alternately, starting with the ridge near the peak of the TP (Fig. 5a). Accordingly, the northerly flows over eastern China [analyzed by Chiang et al. (2020)] can develop between this first ridge and the trough just east of it. This interpretation implies that the northerlies are also explained through Son et al. (2019, 2020). On the other hand, the southerly flow on which Son et al. (2019, 2020) focused is formed between the trough and another ridge farther east of it (so the latter is a manifestation of the intensification of the NPSH).

Figure 7 summarizes the ratio of precipitation averaged over the EASM domain to CTR in each experiment. The maximum EASM precipitation occurs in CTR, which is more than twice that in NoTP and almost equal to that in TPE10 and TPW10. In contrast, the farther west the TP moves, the drier the EASM domain becomes. Nevertheless, TPW30 simulates the rainfall amount similar to that in TPN10 and TPS10. This means that the EASM precipitation is more sensitive to change in the latitudinal location of the TP than the longitudinal location. This is because that when the TP is placed along the path of the jet stream, their interaction is strong enough to form the rainband over the midlatitudes (not necessarily over East Asia); otherwise, the interaction becomes small, and the wave response can be weak. Additionally, the driest case, where the EASM precipitation is approximately 67% less than that in CTR, corresponds to TPN20. It is interesting to note that TPN20 simulates the EASM domain even drier than NoTP.

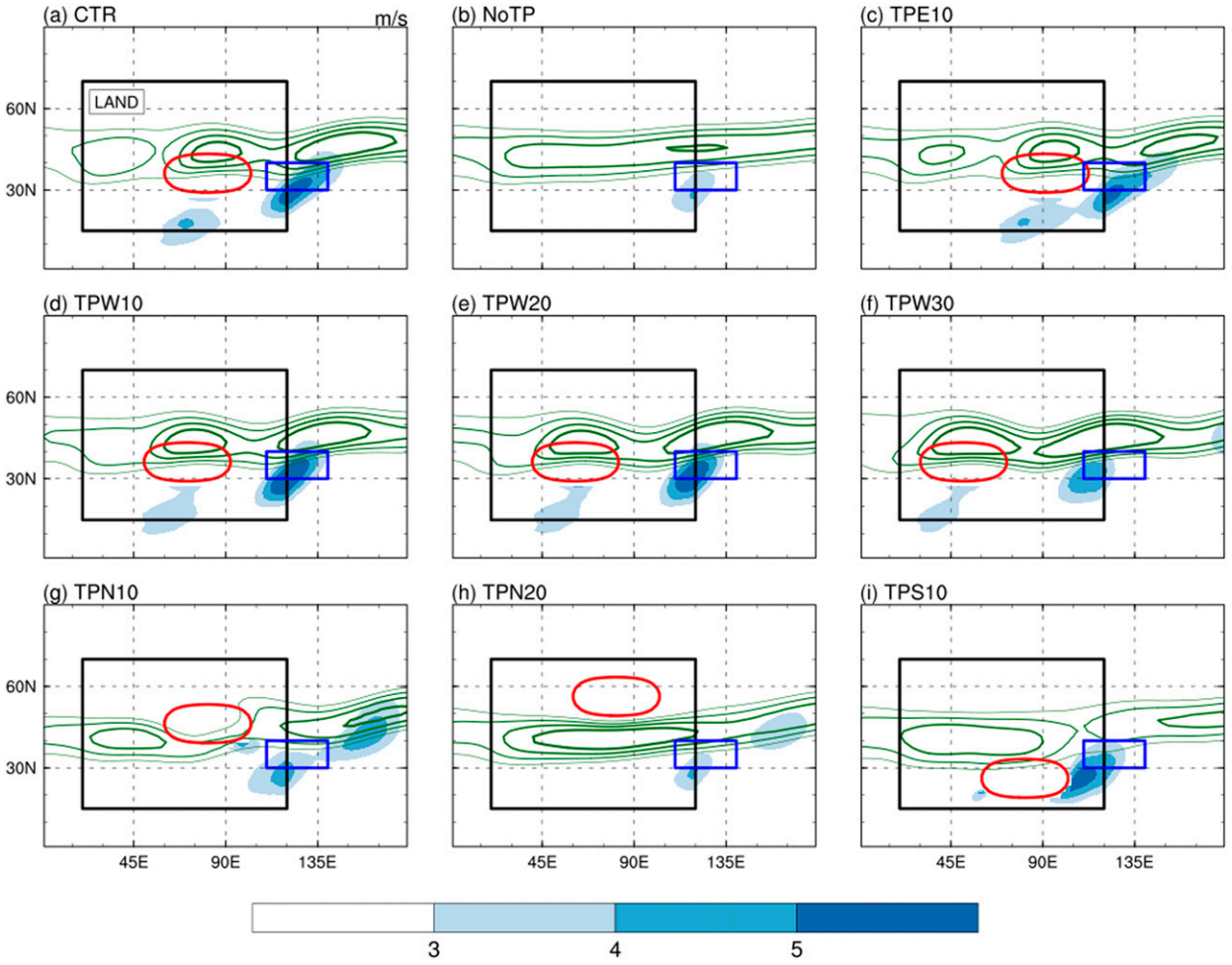

FIG. 6. Meridional wind at 850 hPa (shaded; m s^{-1}) and zonal wind at 200 hPa (green contours; m s^{-1}). The contour levels are 22, 26, 30, and 34 m s^{-1}. The thicker the contour line is, the larger is the speed.

This is probably because the Rossby waves disperse southeastward and then induce an anticyclonic circulation over 90°–120°E at approximately 30°N (not shown).

Above all, we propose that the peak EASM precipitation seems to occur when the TP is situated in the vicinity of its current location. This is also confirmed in our additional experiments in which the Gaussian bell-shaped mountain in CTR, TPE10, and TPW10 is replaced with the realistic topography (not shown). However, more in-depth work is needed to determine the orographic effects on the EASM precipitation because our study is based on idealized simulations. For example, some studies performed model experiments that change the shape of the realistic orography (e.g., extending or removing a part of it) to reveal the role of the TP (Chen et al. 2014; Baldwin and Vecchi 2016; Kong and Chiang 2020). Nevertheless, our result has significant implications for the origin of the EASM, similar to the results of Chiang et al. (2020).

c. *Meridional wind response to the location of the TP*

In the previous section, we confirmed that the EASM precipitation varies drastically with the location of the TP, which might be related to the jet stream. We now perform a detailed examination of how the EASM precipitation is regulated by the location of the TP.

Figure 8 exhibits the difference in precipitation and vertically integrated moisture flux pattern between each experiment and NoTP. As can be seen in Fig. 8a, the presence of the TP allows moisture to be transported from the low latitudes to the midlatitudes, thus producing the EASM precipitation. We infer that this interpretation is also appropriate for TPE10, TPW10, TPW20, and TPW30 because the downstream precipitation pattern induced by the TP is similar in these cases and CTR (Figs. 8a–e). Certainly, the rainband gradually escapes from the EASM region and is diluted with the TP moving inland, but it clearly exists. In other words, as long as the TP moves sideways, it still induces a large amount of moisture transport into the downstream region. However, such a variation is not found in TPN10, TPN20, and TPS10 (Figs. 8f–h). Compared with NoTP, these meridionally displaced cases seem to induce precipitation changes that are mainly confined to the TP rather than the EASM region.

The question then arises as to how the movement of the TP alters the magnitude and location of the EASM precipitation.

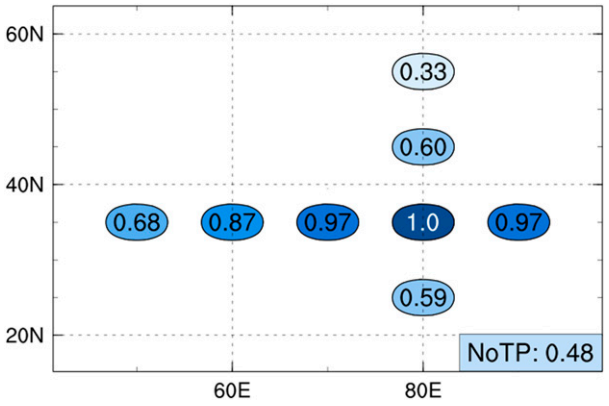

FIG. 7. Ratio of precipitation averaged over the EASM domain to CTR in each experiment.

To answer this question, each wind component is examined separately. First, the low-level zonal wind needs to be checked to determine the change in precipitation. Figure 9 shows 850-hPa zonal wind averaged over 10°–20°N. We could identify that the presence of the TP strengthens the 850-hPa wind substantially in all cases except for TPN20. It is well known that moisture flux converges over the tropics, where the easterlies and westerlies meet, and then turns northward, thereby helping to increase the EASM precipitation (Fig. 8a; Ninomiya and Kobayashi 1999; Kitoh 2004; Sampe and Xie 2010). More notably, the shift of the TP in the east–west direction involves the movement of the wind convergence region where the wind speed is zero (Fig. 9). Therefore, the zonal migration of the TP might cause the rainband to move as well. Conversely, the decrease in the convergence is conspicuous when the TP moves in the north–south direction from its original location. Thus, it is expected that moisture is not sufficient to feed the EASM precipitation in TPN10, TPN20, and TPS10.

We now analyze the longitude–pressure cross section of the meridional wind and eddy geopotential height at 30°N (Fig. 10). The barotropic wind structure is observed in CTR (Fig. 10a), whereas NoTP shows the very weak meridional wind confined to the lower troposphere (Fig. 10b), as previously mentioned (see also Fig. 4). Meanwhile, the TP has a substantial influence even when it moves zonally. This is because the upstream westerly jet still crosses over and interacts strongly with the TP (Fig. 6). This again implies that the westerly jet induces the barotropic Rossby waves resulting from the vertical compression of the air (Son et al. 2019, 2020). However, the southerly winds in TPN10 and TPN20 are considerably weak and not much different from those in NoTP. In TPS10, the presence of the TP slightly enhances the meridional wind, but its effect is mostly confined to the lower levels.

As shown in Fig. 5, the rainband is only observed in five of our experiments (CTR, TPE10, TPW10, TPW20, and TPW30). Therefore, we speculate that the rainband could appear when the southerlies are sufficiently reinforced by the TP (Figs. 5 and 10). TPS10 may be an exception to this, which is addressed further below. We also identify that the wind structure could determine the location and magnitude of the rainband. For example, although the winds are also enhanced in TPW20 and TPW30, the TP forcing affects the area farther west of the EASM domain. As a result, the wind structure is vertically tilted compared with that in CTR (Figs. 10a,e,f). This is the reason why the rainband migrates and weakens with the TP moving inland. In other words, as in CTR, active convection is simulated when the effects of the TP and land–sea distribution happen concurrently in the EASM region.

In contrast, the cross sections in Figs. 10b, 10g, and 10h are similar to each other regardless of the presence or location of the TP because the lower-level winds seen in these experiments are mainly formed from the land–sea thermal contrast. Note that each experiment includes the same land–sea distribution. Furthermore, we confirm that the northward movement of the TP does not provide enough moisture to produce strong precipitation over the EASM region. In TPS10, the downstream southerly flows are intensified but occur near the eastern flank of the TP and do not expand poleward (Figs. 6i and 10i). Additionally, through strong moisture flux convergence in the southern TP, it is conjectured that the TP prevents moisture from being transported to the midlatitudes (not shown, but inferred from Figs. 5i and 8h). Owing to these characteristics, the EASM precipitation is meager in TPS10.

4. Summary and discussion

Using simplified AGCM experiments, we investigate the sensitivity of the EASM precipitation to the location of the TP. By comparing how precipitation develops in each simulation, we can better understand the role of the TP in reinforcing the precipitation. The movement of the TP directly alters the monsoon precipitation system through its impact on meridional winds. The main conclusions are summarized as follows.

First, we show that the uplift of the TP generally leads to increases in the EASM precipitation and the southerly flow. The EASM precipitation could appear when the TP height is at least 80% of the original height. Specifically, we consider the barotropic meridional wind produced by the Tibetan forcing to be a primary factor in the development of the EASM. Next, the strongest EASM precipitation occurs when the TP is situated near its original location. In this case, the impacts of both the TP and land–sea distribution simultaneously induce the southerly flows into the EASM region. This condition is prone to the monsoon development because the winds supply heat and moisture to the EASM region. As such, the fortuitous positioning of the current TP results in favorable conditions for the hydrological cycle over East Asia. Even if the TP is relocated zonally, the slanted rainband still appears because the subtropical jet interacts with the TP. However, the rainband migrates zonally because the Rossby wave response (i.e., a series of troughs and ridges) to the orographic forcing moves so that the strong zonal pressure gradient shifts from the EASM region to other regions.

In contrast, when the TP moves in the latitudinal direction, the EASM precipitation is not very different from that in the no-TP case. Note that the no-TP case simulates the weaker EASM precipitation than the case when the TP is situated at the original location. Moreover, the driest case is simulated

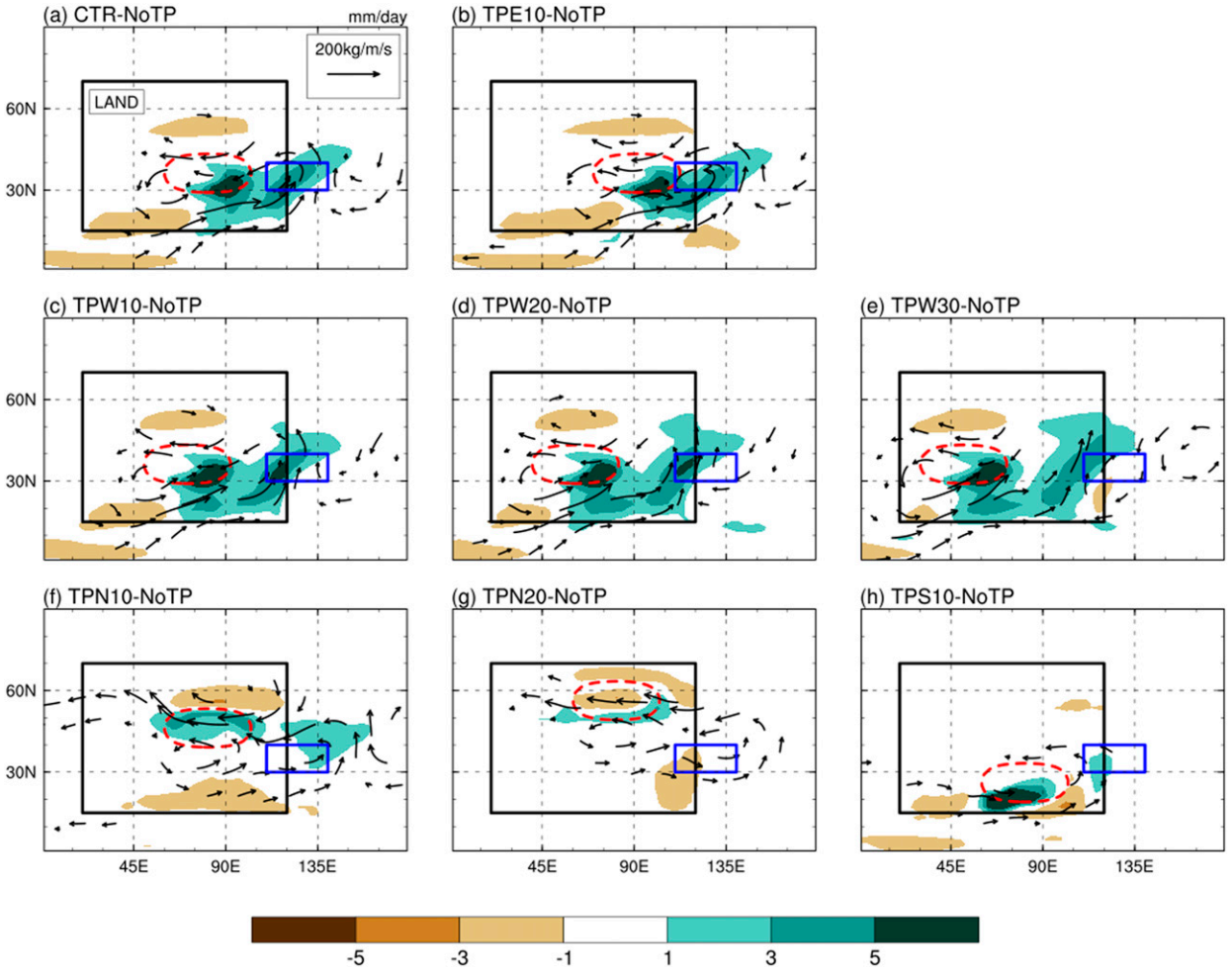

FIG. 8. Difference in precipitation (shaded; mm day^{-1}) and vertically integrated (from p_s to 300 hPa) moisture flux (vectors; kg m^{-1} s^{-1}) between each experiment and NoTP. Magnitude of vectors less than 50 kg m^{-1} s^{-1} is omitted.

when the TP moves to northern Eurasia, and herein only the weak southerlies flow into the EASM region. Thus, it can be inferred that the EASM precipitation is more sensitive to the change in the TP's latitudinal location than the longitudinal location. In this context, our study shows that although the TP currently has a dominant role in the generation of the EASM, the influence varies with its location.

One might ask how the EASM will change in the future based on the relative position of the subtropical jet to the TP because the poleward shift of the jet is expected under the

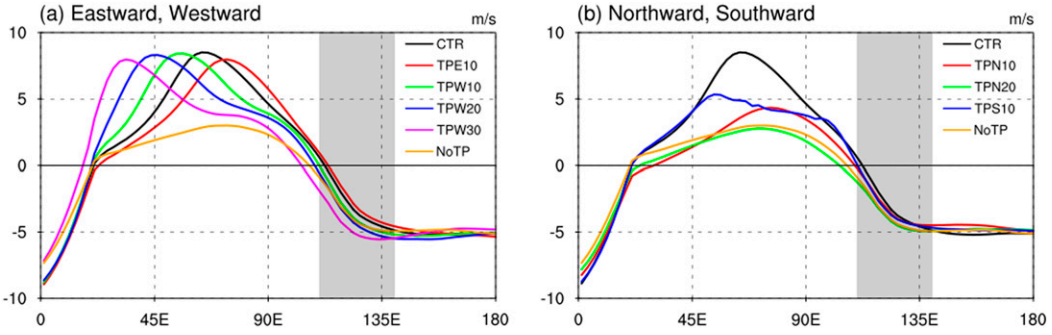

FIG. 9. Zonal wind at 850 hPa (m s^{-1}) averaged over 10°–20°N in each case. The shaded area denotes the longitudinal range of the EASM domain. Positive and negative values represent westerly and easterly winds, respectively. The CTR and NoTP cases are also illustrated in both figures.

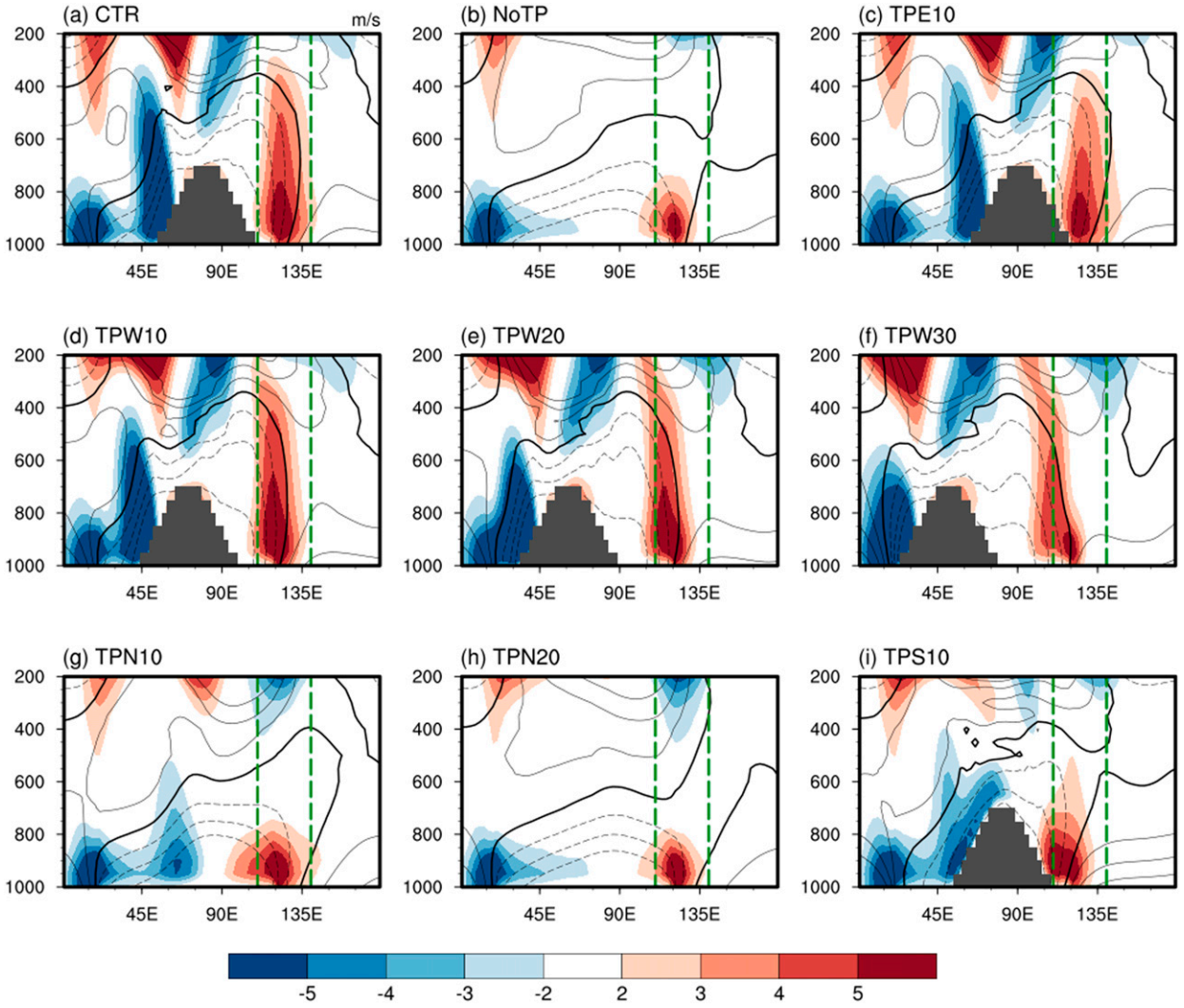

FIG. 10. Longitude–pressure cross section of meridional wind (shaded; m s^{-1}) and eddy geopotential height (contour interval 20 gpm) along 30°N. The zero contour is thickened, and the green vertical dashed lines denote the boundary of the EASM domain.

warming climate (Lu et al. 2007; Fu and Lin 2011). There is a high probability that the EASM both begins and terminates earlier than in the present climate because of the jet's poleward shift. Many studies proposed that the overall phase of the EASM is determined by the meridional position of the westerly jet, which moves from south to north of the TP with its seasonal transition (Molnar et al. 2010; Chiang et al. 2020; Kong and Chiang 2020). In this sense, it is plausible that the northward transition of the westerly jet hastens the monsoon period itself. This conjecture is also consistent with the results of Son et al. (2020), who showed that the upstream speed of the westerly jet may determine the intraseasonal evolution of the monsoon cycle. For example, if the latitudinal location of the upstream jet stream core is collocated with the TP center, then the Rossby wave response is greatest, and thus the EASM rainfall can increase. Accordingly, a northward shift of the jet can be interpreted as a weakening of the wave response, causing the earlier retreat of the monsoon. However, this analysis is based only on the position of the jet, and more factors that affect the EASM in the (intra)seasonal time scales should be considered for further discussion.

Meanwhile, our idealized experiment is designed to capture the EASM, but we expect that it could also describe other monsoon systems such as the Indian summer monsoon and South American summer monsoon by modifying orographic configurations. A more detailed discussion on this topic will be presented in the future. In conclusion, we hope that this study improves understanding of the role of the TP in modulating the EASM.

Acknowledgments. This work was supported by the Korea Meteorological Administration (KMA) Research and Development Program under Grant KMI2021–01410. We appreciate the three anonymous reviewers for their helpful and constructive comments, which have improved the paper.

REFERENCES

Abe, M., A. Kitoh, and T. Yasunari, 2003: An evolution of the Asian summer monsoon associated with mountain uplift—Simulation with the MRI atmosphere–ocean coupled GCM. *J. Meteor. Soc. Japan*, **81**, 909–933, https://doi.org/10.2151/jmsj.81.909.

Adler, R. F., and Coauthors, 2003: The version-2 Global Precipitation Climatology Project (GPCP) monthly precipitation analysis (1979–present). *J. Hydrometeor.*, **4**, 1147–1167, https://doi.org/10.1175/1525-7541(2003)004<1147:TVGPCP>2.0.CO;2.

An, Z., J. E. Kutzbach, W. L. Prell, and S. C. Porter, 2001: Evolution of Asian monsoons and phased uplift of the Himalaya–Tibetan plateau since Late Miocene times. *Nature*, **411**, 62–66, https://doi.org/10.1038/35075035.

Anderson, J. L., and Coauthors, 2004: The new GFDL global atmosphere and land model AM2–LM2: Evaluation with prescribed SST simulations. *J. Climate*, **17**, 4641–4673, https://doi.org/10.1175/JCLI-3223.1.

Baldwin, J., and G. Vecchi, 2016: Influence of the Tian Shan on arid extratropical Asia. *J. Climate*, **29**, 5741–5762, https://doi.org/10.1175/JCLI-D-15-0490.1.

Chen, G. S., Z. Liu, and J. E. Kutzbach, 2014: Reexamining the barrier effect of the Tibetan Plateau on the South Asian summer monsoon. *Climate Past*, **10**, 1269–1275, https://doi.org/10.5194/cp-10-1269-2014.

Chen, J., and S. Bordoni, 2014: Orographic effects of the Tibetan Plateau on the East Asian summer monsoon: An energetic perspective. *J. Climate*, **27**, 3052–3072, https://doi.org/10.1175/JCLI-D-13-00479.1.

Chiang, J. C. H., W. Kong, C. H. Wu, and D. S. Battisti, 2020: Origins of East Asian summer monsoon seasonality. *J. Climate*, **33**, 7945–7965, https://doi.org/10.1175/JCLI-D-19-0888.1.

Chou, C., 2003: Land–sea heating contrast in an idealized Asian summer monsoon. *Climate Dyn.*, **21**, 11–25, https://doi.org/10.1007/s00382-003-0315-7.

Ding, Y., and J. C. L. Chan, 2005: The East Asian summer monsoon: An overview. *Meteor. Atmos. Phys.*, **89**, 117–142, https://doi.org/10.1007/s00703-005-0125-z.

Duan, A., R. Sun, and J. He, 2017: Impact of surface sensible heating over the Tibetan Plateau on the western Pacific subtropical high: A land–air–sea interaction perspective. *Adv. Atmos. Sci.*, **34**, 157–168, https://doi.org/10.1007/s00376-016-6008-z.

Fu, Q., and P. Lin, 2011: Poleward shift of subtropical jets inferred from satellite-observed lower-stratospheric temperatures. *J. Climate*, **24**, 5597–5603, https://doi.org/10.1175/JCLI-D-11-00027.1.

Hahn, D. G., and S. Manabe, 1975: The role of mountains in the South Asian monsoon circulation. *J. Atmos. Sci.*, **32**, 1515–1541, https://doi.org/10.1175/1520-0469(1975)032<1515:TROMIT>2.0.CO;2.

Held, I. M., 1983: Stationary and quasi-stationary eddies in the extratropical troposphere: Theory. *Large-Scale Dynamical Processes in the Atmosphere*, B. J. Hoskins and R. P. Pearce, Eds., Academic Press, 127–168.

Kitoh, A., 2004: Effects of mountain uplift on East Asian summer climate investigated by a coupled atmosphere–ocean GCM. *J. Climate*, **17**, 783–802, https://doi.org/10.1175/1520-0442(2004)017<0783:EOMUOE>2.0.CO;2.

Kong, W., and J. C. H. Chiang, 2020: Interaction of the westerlies with the Tibetan Plateau in determining the mei-yu termination. *J. Climate*, **33**, 339–363, https://doi.org/10.1175/JCLI-D-19-0319.1.

Kutzbach, J. E., W. L. Prell, and W. F. Ruddiman, 1993: Sensitivity of Eurasian climate to surface uplift of the Tibetan Plateau. *J. Geol.*, **101**, 177–190, https://doi.org/10.1086/648215.

Lee, J.-Y., B. Wang, K.-H. Seo, K.-J. Ha, A. Kitoh, and J. Liu, 2015: Effects of mountain uplift on global monsoon precipitation. *Asia-Pac. J. Atmos. Sci.*, **51**, 275–290, https://doi.org/10.1007/s13143-015-0077-2.

Lin, S.-J., 2004: A ''vertically Lagrangian'' finite-volume dynamical core for global models. *Mon. Wea. Rev.*, **132**, 2293–2307, https://doi.org/10.1175/1520-0493(2004)132<2293:AVLFDC>2.0.CO;2.

Lin, Z., and R. Lu, 2008: Abrupt northward jump of the East Asian upper-tropospheric jet stream in mid-summer. *J. Meteor. Soc. Japan*, **86**, 857–866, https://doi.org/10.2151/jmsj.86.857.

Liu, X., and Z.-Y. Yin, 2002: Sensitivity of East Asian monsoon climate to the uplift of the Tibetan Plateau. *Palaeogeogr. Palaeoclimatol. Palaeoecol.*, **183**, 223–245, https://doi.org/10.1016/S0031-0182(01)00488-6.

Liu, Y., B. Hoskins, and M. Blackburn, 2007: Impact of Tibetan orography and heating on the summer flow over Asia. *J. Meteor. Soc. Japan*, **85B**, 1–19, https://doi.org/10.2151/jmsj.85.1.

Lu, J., G. A. Vecchi, and T. Reichler, 2007: Expansion of the Hadley cell under global warming. *Geophys. Res. Lett.*, **34**, L06805, https://doi.org/10.1029/2006GL028443.

Manabe, S., and A. J. Broccoli, 1990: Mountains and arid climates of middle latitudes. *Science*, **247**, 192–195, https://doi.org/10.1126/science.247.4939.192.

Miyasaka, T., and H. Nakamura, 2005: Structure and formation mechanisms of the Northern Hemisphere summertime subtropical highs. *J. Climate*, **18**, 5046–5065, https://doi.org/10.1175/JCLI3599.1.

Molnar, P., P. England, and J. Martinod, 1993: Mantle dynamics, uplift of the Tibetan Plateau, and the Indian monsoon. *Rev. Geophys.*, **31**, 357–396, https://doi.org/10.1029/93RG02030.

——, W. R. Boos, and D. S. Battisti, 2010: Orographic controls on climate and paleoclimate of Asia: Thermal and mechanical roles for the Tibetan Plateau. *Annu. Rev. Earth Planet. Sci.*, **38**, 77–102, https://doi.org/10.1146/annurev-earth-040809-152456.

Ninomiya, K., and C. Kobayashi, 1999: Precipitation and moisture balance of the Asian summer monsoon in 1991. *J. Meteor. Soc. Japan*, **77**, 77–99, https://doi.org/10.2151/jmsj1965.77.1_77.

Okajima, H., and S.-P. Xie, 2007: Orographic effects on the northwestern Pacific monsoon: Role of air–sea interaction. *Geophys. Res. Lett.*, **34**, L21708, https://doi.org/10.1029/2007GL032206.

Park, H.-S., J. C. H. Chiang, and S. Bordoni, 2012: The mechanical impact of the Tibetan Plateau on the seasonal evolution of the South Asian monsoon. *J. Climate*, **25**, 2394–2407, https://doi.org/10.1175/JCLI-D-11-00281.1.

Reynolds, R. W., N. A. Rayner, T. M. Smith, D. C. Stokes, and W. Wang, 2002: An improved in situ and satellite SST analysis for climate. *J. Climate*, **15**, 1609–1625, https://doi.org/10.1175/1520-0442(2002)015<1609:AIISAS>2.0.CO;2.

Ringler, T. D., and K. H. Cook, 1995: Orographically induced stationary waves: Dependence on latitude. *J. Atmos. Sci.*, **52**, 2548–2560, https://doi.org/10.1175/1520-0469(1995)052<2548:OISWDO>2.0.CO;2.

——, and ——, 1999: Understanding the seasonality of orographically forced stationary waves: Interaction between mechanical and thermal forcing. *J. Atmos. Sci.*, **56**, 1154–1174, https://doi.org/10.1175/1520-0469(1999)056<1154:UTSOOF>2.0.CO;2.

Rodwell, M. J., and B. J. Hoskins, 2001: Subtropical anticyclones and summer monsoons. *J. Climate*, **14**, 3192–3211, https://doi.org/10.1175/1520-0442(2001)014<3192:SAASM>2.0.CO;2.

Sampe, T., and S.-P. Xie, 2010: Large-scale dynamics of the meiyu-baiu rainband: Environmental forcing by the westerly jet. *J. Climate*, **23**, 113–134, https://doi.org/10.1175/2009JCLI3128.1.

Sato, T., 2009: Influences of subtropical jet and Tibetan Plateau on precipitation pattern in Asia: Insights from regional climate modeling. *Quat. Int.*, **194**, 148–158, https://doi.org/10.1016/j.quaint.2008.07.008.

Seo, K.-H., J.-H. Son, and J.-Y. Lee, 2011: A new look at changma (in Korean with English abstract). *Atmosphere*, **21**, 109–121, https://doi.org/10.14191/Atmos.2011.21.1.109.

——, ——, ——, and H.-S. Park, 2015: Northern East Asian monsoon precipitation revealed by airmass variability and its prediction. *J. Climate*, **28**, 6221–6233, https://doi.org/10.1175/JCLI-D-14-00526.1.

Son, J.-H., K.-H. Seo, and B. Wang, 2019: Dynamical control of the Tibetan Plateau on the East Asian summer monsoon. *Geophys. Res. Lett.*, **46**, 7672–7679, https://doi.org/10.1029/2019GL083104.

——, ——, and ——, 2020: How does the Tibetan Plateau dynamically affect downstream monsoon precipitation? *Geophys. Res. Lett.*, **47**, e2020GL090543, https://doi.org/10.1029/2020GL090543.

Wang, B., Q. Bao, B. Hoskins, G. Wu, and Y. Liu, 2008: Tibetan Plateau warming and precipitation changes in East Asia. *Geophys. Res. Lett.*, **35**, L14702, https://doi.org/10.1029/2008GL034330.

Wu, G., and Coauthors, 2007: The influence of mechanical and thermal forcing by the Tibetan Plateau on Asian climate. *J. Hydrometeor.*, **8**, 770–789, https://doi.org/10.1175/JHM609.1.

——, Y. Liu, B. Dong, X. Liang, A. Duan, Q. Bao, and J. Yu, 2012: Revisiting Asian monsoon formation and change associated with Tibetan Plateau forcing: I. Formation. *Climate Dyn.*, **39**, 1169–1181, https://doi.org/10.1007/s00382-012-1334-z.

Zhang, Y., X. Kuang, W. Guo, and T. Zhou, 2006: Seasonal evolution of the upper-tropospheric westerly jet core over East Asia. *Geophys. Res. Lett.*, **33**, 2006GL026377, https://doi.org/10.1029/2006GL026377.